Polyhedron 29 (2010) 2924–2932

Contents lists available at ScienceDirect

Polyhedron

journal homepage: www.elsevier.com/locate/poly

ONN-complexes of dioxomolybdenum(VI) with 2-hydroxy-1-naphthaldehyde S-ethyl-4-H/phenyl-thiosemicarbazones: Crystal structure, electrochemistry and *in situ* spectroelectrochemistry

Songül Duman [a], İrfan Kızılcıklı [a], Atıf Koca [b], Mehmet Akkurt [c], Bahri Ülküseven [a,*]

[a] Department of Chemistry, Istanbul University, 34320 Avcılar, Istanbul, Turkey
[b] Department of Chemical Engineering, Faculty of Engineering, Marmara University, Göztepe 34722, Istanbul, Turkey
[c] Department of Physics, Erciyes University, Faculty of Arts and Sciences, 38039 Kayseri, Turkey

ARTICLE INFO

Article history:
Received 13 April 2010
Accepted 17 July 2010
Available online 6 August 2010

Keywords:
Thiosemicarbazone
Dioxomolybdenum complex
Structural analysis
Cyclic voltammetry
Spectroelectrochemical analysis

ABSTRACT

Neutral dioxomolybdenum(VI) complexes of dibasic 2-hydroxy-1-naphthaldehyde S-ethyl-4-H/phenyl-thiosemicarbazones (H: **L^1**, C_6H_5: **L^2**) have been synthesized. The complexes, $[MoO_2L^I(ROH)]$ (**1a–d**) and $[MoO_2L^{II}(ROH)]$ (**2a–d**) (R: CH_3, C_2H_5, C_3H_7, C_4H_9) were characterized by elemental analysis, electronic, IR and ^{1}H NMR spectra. X-ray crystal studies indicated a distorted octahedral geometry for $[MoO_2(L^1)(C_2H_5OH)]$ (**1b**) and $[MoO_2(L^2)(CH_3OH)]$ (**2a**). The Mo–O bond lengths of the MoO_2^{2+} moieties are almost the same in the monoclinic crystal structures of complexes **1b** and **2a**, and the MoO_2 cores have a *cis*-dioxomolybdenum structure with angles *ca.* 105 Å. While **1b** crystallizes in the space group C2/c, **2a** crystallizes in the space group $P2_1/n$. The electrochemical behaviors of the ligands and their complexes **1b** and **2a** were studied using cyclic voltammetry and square wave voltammetry. The half-wave potentials ($E_{1/2}$) are significantly influenced by the central metal ions, the nature of the substituents on the thiosemicarbazones, and the electronic character of the ligands, which are the important factors that control redox potentials. *In situ* spectroelectrochemical studies were employed to determine the spectra of the electrogenerated species of the complexes and to assign the redox processes. The colors of the electrogenerated species were determined with *in situ* electrocolorimetric measurements.

1. Introduction

Molybdenum is a trace element and one of the cofactors for several enzymes catalyzing redox reactions [1,2], and some molybdenum compounds are included in plausible enzyme model systems [3–5]. Mixed ligand complexes with a MoO_2^{2+} core and having the general formula $[MoO_2(L)(L')]$ were synthesized as model systems of molybdoenzymes catalyzing redox reactions. The catalytic capacity of the molybdenum compounds has been thought to be related to the structural features of the chelated *cis*-MoO_2 unit [1]. Additionally, the relationships between the catalytic activity of the complexes and their chelate ring structure and also the substituents of the ligands have been examined [6,7].

Many thiosemicarbazones show various biological activities. The known molybdenum(VI) complexes of thiosemicarbazones of the general formula $[MoO_2L(L')]$ are potential catalysts as the coordinated L′ molecule may be replaced by an activated enzyme molecule. Chelate complexes with a *cis*-MoO_2 center have been synthesized for oxygen atom transfer (OAT) reactions and progress towards this objective is continues to increase. In the last 20 years, a large number of dioxomolybdenum complexes with different ligand types having O_2N [8,5], S_2ON [3], SO_2N_2 [9], O_2N_2 [10], S_2N_2 [11] or ONS [12] donor sets have been synthesized, and their activities for catalyzing an OAT reaction were reported [13]. For this purpose, structural analysis of dioxomolybdenum complexes of the general formula $[MoO_2(L)(L')]$ have been studied using various dibasic 2-hydroxy-arilydene-S-alkylthiosemicarbazones. These papers report that the sulfur [14–16], N^4-nitrogen [13,4,17–19] monosubstitued, and sulfur and N^4-nitrogen [20–22] disubstitued thiosemicarbazone derivatives act as ONN or ONS donor sets.

In this work, we have used two S-ethyl 4-H/phenyl-thiosemicarbazones (H_2L^1 and H_2L^2) to determine the structural and electrochemical properties of dioxomolybdenum complexes of the composition $[MoO_2L(L')]$, the second ligand (L′) was a C_{1-4} *n*-alcohol (Fig. 1). *In situ* spectroelectrochemical and *in situ* electrocolorimetric studies were employed for the first time to determine the spectra and colors of the electrogenerated species of the dioxomolybdenum(VI) complexes.

* Corresponding author.
E-mail address: bahseven@istanbul.edu.tr (B. Ülküseven).

0277-5387/$ - see front matter © 2010 Elsevier Ltd. All rights reserved.
doi:10.1016/j.poly.2010.07.022

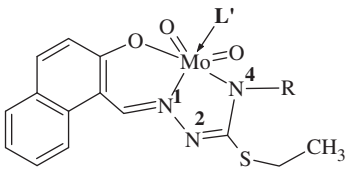

Fig. 1. The thiosemicarbazones. R: H (**L**[1]), C_6H_5 (**L**[2]). The molybdenum complexes. L′: CH_3OH (**1a** and **2a**), C_2H_5OH (**1b** and **2b**), C_3H_7OH (**1c** and **2c**), C_4H_9OH (**1d** and **2d**).

2. Experimental

2.1. IR and ^{1}H NMR data

The elemental analyses were determined on a Thermo Finnigan Flash EA 1112 Series Elemantar Analyser. Infrared spectra were recorded as KBr discs on a Mattson 1000 FT-IR spectrophotometer in the 4000–400 cm^{-1} range at room temperature. The ^{1}H NMR spectra were recorded on Bruker Avance-500 model spectrometer relative to $SiMe_4$ using $CDCl_3$.

2.2. X-ray structure determination

Single crystal data collection for the complexes was performed on a Rigaku RAXIS RAPID imaging plate area detector with graphite monochromated Mo Kα radiation. The data were collected at a temperature of 295(2) K to a maximum 2θ value of 60.3°. A total of 144 oscillation images for **1b** and 135 oscillation images for **2a** were collected. A sweep of data was done using ω oscillations from 0.0° to 180.0° in 5.0° steps for **1b** and in 4.0° steps for **2a**. The exposure rate was 48.0 [s/°] for **1b** and 30.0 [s/°] for **2a**. The detector swing angle was 0.03° for **1b** and 0.02° for **2a**. CrystalClear [23] and SORTAV [24] were used for the cell refinement and data reduction. The crystal structures were solved by means of direct methods using SIR-97 [25], while the refinement and all further calculations were carried out using SHELXL-97 [26]. ORTEP-3 for Windows [27] and PLATON [28] were used for molecular graphics. For **1b**, the H atom H1 of the OH group was located from a difference Fourier map, and its isotropic thermal parameter was constrained to ride on O4 with $U_{iso}(H) = 1.5U_{eq}(O)$. The other H atoms were positioned with an idealized geometry using a riding model with C–H = 0.93–0.97 Å, N–H = 0.86 Å and $U_{iso}(H) = 1.2U_{eq}(C,N)$. The C and H atoms of the ethanol moiety exhibit disorder over two positions. The site occupancies for the disordered part refined to 0.771(13) and 0.229(13). For **2a**, The H atom H1 of the OH group was located from a difference Fourier map, and its isotropic thermal parameter was constrained to ride on O4 with $U_{iso}(H) = 1.5U_{eq}(O)$. The other H atoms were positioned with an idealized geometry using a riding model with C–H = 0.93–0.97 Å, N–H = 0.86 Å and $U_{iso}(H) = 1.2U_{eq}(C,N)$. The non-H atoms were refined anisotropically, using weighted full-matrix least-squares on F^2. The crystal data and refinement details are presented in Tables 1–4.

2.3. Electrochemistry and spectroelectrochemistry

The measurements were carried out with a Gamry Reference 600 potentiostat/galvanostat utilizing a three-electrode configuration at 25 °C. For cyclic voltammetry (CV) and square wave voltammetry (SWV) measurements, the working electrode was a Pt disc with a surface area of 0.071 cm^2. The surface of the working electrode was polished with a diamond suspension before each run. A Pt wire served as the counter electrode. A saturated calomel electrode (SCE) was employed as the reference electrode and separated from the bulk of the solution by a double bridge. Ferrocene was used as an internal reference. Tetrabutylammonium perchlorate (TBAP) in dichloromethane (DCM) was employed as the supporting electrolyte at a concentration of 0.10 mol dm^{-3}. High purity N_2 was used to remove dissolved O_2 at least 15 min prior to each run and to maintain a nitrogen blanket during the measurements. IR

Table 1
The crystallographic data and structure refinement for complexes **1b** and **2a**.

Compound	**1b**	**2a**
Formula	$C_{16}H_{19}MoN_3O_4S$	$C_{21}H_{21}MoN_3O_4S$
Formula Weight	445.35	507.41
Crystal system	monoclinic	monoclinic
Space Group	*C*2/*c*	$P2_1/n$
Unit cell dimension		
a (Å)	28.3766 (5)	10.8830 (2)
b (Å)	8.3090 (1)	8.1727 (1)
c (Å)	19.7391 (6)	24.0848 (5)
α (°)	90	90
β (°)	129.282 (2)	93.747 (1)
γ (°)	90	90
V (Å^3)	3602.46 (17)	2137.61 (6)
Z	8	4
ρ_{calc} (g cm^{-3})	1.642	1.577
μ(Mo Kα) (mm^{-1})	0.87	0.74
F(0 0 0)	1808	1032
Crystal size (mm)	0.20 × 0.20 × 0.50	0.20 × 0.20 × 0.50
Crystal shape, crystal color	prism, red	block, red
T (K)	295(2)	295(2)
λ (Mo Kα) (Å)	0.71073	0.71073
θ Range (°)	2.60–30.12	3.00–30.17
h, *k*, *l* limits	−40: 39, −11: 10, −27: 27	−15: 15, −11: 11, −31: 33
Reflections: total, unique data, R_{int}	64 882, 5200, 0.026	61 397, 6236, 0.033
Observed data [$I > 2\sigma(I)$]	5123	6019
T_{min}, T_{max}	0.812, 0.840	0.836, 0.862
N_{ref}, N_{par}	5123, 262	6019, 277
R_1, wR_2, *S* [$I > 2\sigma(I)$]	0.0260, 0.074, 1.04	0.033, 0.090, 1.04
Weighting scheme	$w = 1/[\sigma^2(F_o^2) + (0.046P)^2 + 2.6614P]$ where $P = (F_o^2 + 2F_c^2)/3$	$w = 1/[\sigma^2(F_o^2) + (0.0532P)^2 + 0.8659P]$ where $P = (F_o^2 + 2F_c^2)/3$
Largest difference in peak and hole (e Å^{-3})	0.45, −0.88	1.01, −0.48

Table 2
The molybdenum centered bond distances of **1b** and **2a** (Å).

1b		2a	
Mo1–O1	1.9447 (17)	Mo1–O1	1.9496 (14)
Mo1–O2	1.6847 (15)	Mo1–O2	1.7049 (14)
Mo1–O3	1.7131 (13)	Mo1–O3	1.6919 (15)
Mo1–O4	2.3727 (13)	Mo1–O4	2.4040 (14)
Mo1–N1	2.2333 (13)	Mo1–N1	2.2201 (14)
Mo1–N3	2.0505 (17)	Mo1–N3	2.0746 (15)

Table 3
The molybdenum centered angle values of **1b** and **2a** (°).

1b		2a	
O1–Mo1–O2	97.82 (8)	O1–Mo1–O2	104.56 (6)
O1–Mo1–O3	106.46 (7)	O1–Mo1–O3	99.03 (8)
O1–Mo1–O4	78.32 (6)	O1–Mo1–O4	77.20 (6)
O1–Mo1–N1	80.47 (5)	O1–Mo1–N1	80.81 (5)
O1–Mo1–N3	147.24 (6)	O1–Mo1–N3	147.49 (6)
O2–Mo1–O3	105.29 (7)	O2–Mo1–O3	105.94 (8)
O2–Mo1–O4	171.74 (7)	O2–Mo1–O4	81.68 (6)
O2–Mo1–N1	93.57 (6)	O2–Mo1–N1	156.31 (6)
O2–Mo1–N3	99.78 (8)	O2–Mo1–N3	95.20 (6)
O3–Mo1–O4	82.87 (6)	O3–Mo1–O4	172.22 (7)
O3–Mo1–N1	158.52 (6)	O3–Mo1–N1	95.74 (7)
O3–Mo1–N3	95.23 (7)	O3–Mo1–N3	100.02 (7)
O4–Mo1–N1	78.65 (5)	O4–Mo1–N1	77.02 (5)
O4–Mo1–N3	80.42 (6)	O4–Mo1–N3	80.51 (5)
N1–Mo1–N3	71.08 (6)	N1–Mo1–N3	71.28 (5)
Mo1–O1–C9	132.99 (12)	Mo1–O1–C9	135.63 (12)
Mo1–O4–C15A	124.9 (2)	Mo1–O4–C12	126.27 (13)
Mo1–O4–C15B	123.8 (10)	Mo1–N1–N2	118.07 (10)
Mo1–N1–C11	126.19 (11)	Mo1–N1–C11	126.20 (11)
Mo1–N1–N2	117.58 (11)	Mo1–N3–C13	119.06 (11)
Mo1–N3–C12	119.69 (14)	Mo1–N3–C16	120.23 (11)

Table 4
Hydrogen bond parameters (Å and °) for **1b** and **2a**.

Complex	D–H···A	*d*(D–H)	*d*(H···A)	*d*(D···A)	<(DHA)
1b	O4–H1···N2^{i}	0.77 (3)	2.02 (3)	2.7855 (18)	177 (4)
	N3–H3A···O3^{ii}	0.86	2.25	3.027 (3)	151
	C13–H13B···O3^{ii}	0.97	2.50	3.324 (2)	143
	O4–H1···Cg1^{iii}	0.77 (3)	2.65 (3)	2.6720 (15)	84 (2)
	C14–H14C···Cg4^{i}	0.96	2.89	3.759 (3)	152
2a	O4–H1···N2^{i}	0.77 (3)	1.99 (3)	2.752 (2)	170 (4)
	C5–H5···Cg5^{ii}	0.93	2.99	3.762 (2)	141
	C15–H15C···Cg3^{iii}	0.96	2.91	3.729 (3)	144

Symmetry codes: (i) $1-x, 1-y, 2-z$; (ii) $1-x, y, 3/2-z$; (iii) x, y, z. Cg1 and Cg4 are the centroids of the Mo1/N1–N3/C12 and C1/C6–C10 rings, respectively.
Symmetry codes: (i) $1-x, -y, 2-z$; (ii) $1/2+x, 1/2-y, -1/2+z$; (iii) $1-x, 1-y, 2-z$. Cg3 and Cg5 are the centroids of the C1–C6 and C16–C21 rings, respectively.

compensation was applied to the CV and SWV scans to minimize the potential control error.

UV–Vis absorption spectra and chromaticity diagrams were measured by an OceanOptics QE65000 diode array spectrophotometer. *In situ* spectroelectrochemical and *in situ* electrocolorimetric measurements were carried out utilizing a three-electrode configuration of a thin-layer quartz spectroelectrochemical cell at 25 °C. The working electrode was a Pt tulle. A Pt wire counter electrode and a SCE reference electrode separated from the bulk of the solution by a double bridge were also used. The standard illuminant A with a 2° observer at constant temperature in a light booth designed to exclude external light was used. Prior to each set of measurements, background color coordinates (x, y and z values) were taken at open-circuit, using the electrolyte solution without the MPc under study. During the measurements, readings were taken as a function of time under kinetic control.

2.4. Syntheses of the compounds

2-Hydroxy-1-naphthaldehyde-S-ethyl-4-H/phenyl-thiosemicarbazones ($\mathbf{L^1}$ and $\mathbf{L^2}$) were synthesized by a known procedure [29,30]. Hydrobromide forms of the ligands, L·HBr, were dissolved in 5 mL ethanol and neutralized with a sufficient amount of aqueous $NaHCO_3$ solution (10%, w/w). The colors, m.p. (°C), yields, microanalysis, FT-IR (KBr, cm^{-1}) and ^1H NMR (500 MHz, $CDCl_3$, 25 °C, δ ppm) data of the ligands are given as follows:

H_2L^1: Light yellow, 172.4, 185 mg (78%). *Anal.* Calc. for $C_{14}H_{15}N_3OS$ (273.35 g/mol): C, 61.51; H, 5.53; N, 15.37; S, 11.73. Found: C, 61.71; H, 5.49; N, 15.30; S, 11.96%. IR: ν(OH) 3110, $\nu_s(NH_2)$ 3310, $\nu_{as}(NH_2)$ 3414, $\delta(NH_2)$ 1651, $\nu(C{=}N^1)$ 1620, $\nu(C{=}N^2)$ 1562. ^1H NMR: 13.00, 12.86 (s, *cis*/*trans*: 1/2, 1H, O*H*), 9.38, 9.26 (s, *syn*/*anti*: 1/1, 1H, C*H*=N^1), 7.19–8.14 (doublet and triplets, 6H, $C_{10}H_6$), 5.11, 4.78 (broad s, *cis*/*trans*: 1/2, 2H, N^4H_2), 3.15, 3.01 (q, *cis*/*trans*: 1/2, 2H, S–CH_2), 1.44, 1.42 (t, *cis*/*trans*: 1/2, 3H, –CH_3).

H_2L^2: Light yellow, 161, 215 mg (62%). *Anal.* Calc. for $C_{20}H_{19}N_3OS$ (349.45 g/mol): C, 68.74; H, 5.48; N, 12.02; S, 9.18. Found: C, 68.52; H, 5.57; N, 11.82; S, 8.92%. IR: ν(OH) 3480, ν(NH) 3410, δ(NH) 1620, $\nu(C{=}N^1)$ 1601, $\nu(C{=}N^2)$ 1562. ^1H NMR: 13.34, 12.73 (s, *cis*/*trans*: 1/2, 1H, O*H*), 9.67, 9.42 (s, d, *syn*/*anti*: 1/1, 1H, C*H*=N^1), 7.32–8.18 (doublet and triplets, 6H, $C_{10}H_6$), 6.34 (broad s, 1H, N^4H), 7.10–7.43 (m, 5H, $N^4C_6H_5$), 3.13, 3.05 (q, *cis*/*trans*: 1/2, 2H, S–CH_2), 1.43, 1.38 (t, *cis*/*trans*: 1/2, 3H, –CH_3).

Preparation of the dioxomolybdenum complexes (**1a–d** and **2a–d**) were realized with small modifications of the procedures reported in the literature [31,32].

1a: The ligand, H_2L^1 (0.27 g, 1.0 mmol) was dissolved in absolute methanol (5.0 mL) by heating. The hot solution was treated with 2.0 mL of a methanolic solution of $MoO_2(acac)_2$ (0.36 g, 1.1 mmol). The reaction mixture was stirred at 60 °C for 4 h and then allowed to stand at room temperature overnight. The cardinal red precipitate (complex **1a**) was collected by filtration and washed twice with 2–4 mL of cold methanol. Recrystallization of the product from ethanol gave the analytical grade pure compound. The crystalline powder was dried for 12 h in air.

The other molybdenum complexes, **1b–d** and **2a–d**, were synthesized by a similar procedure, and recrystallization of the complexes was carried out in alcohol, which is present as a second ligand in the structure.

The air-dried samples of the complexes were used for all analyses. The color, m.p. (°C), yields, microanalysis, FT-IR (KBr, cm^{-1}) and ^1H NMR (500 MHz, $CDCl_3$, 25 °C, δ ppm) data are given below:

1a: Cardinal red, >250 (dec), 155 mg (36%). *Anal.* Calc. for $C_{15}H_{17}MoN_3O_4S$ (431.32 g/mol): C, 41.77; H, 3.97; N, 9.74; S, 7.43. Found: C, 41.81; H, 4.16; N, 9.51; S, 7.13%. IR: ν(OH) 3434, ν(NH) 3226, δ(NH) 1616, $\nu(C{=}N^1)$ 1597, $\nu(C{=}N^2)$ 1547, ν_s,ν_{as} (MoO_2) 955, 912. ^1H NMR: 9.74 (s, 1H, C*H*=N^1), 7.34–8.27 (doublet and triplets, 6H, $C_{10}H_6$), 7.08 (s, 1H, N^4H), 3.21 (q, 2H, S–CH_2), 1.45 (t, 3H, –CH_3), 3.49 (s, 3H, –C$^1H_3$).

1b: Cardinal red, >250 (dec), 380 mg (85%). *Anal.* Calc. for $C_{16}H_{19}MoN_3O_4S$ (445.35 g/mol): C, 43.15; H, 4.30; N, 9.44; S, 7.20. Found: C, 43.66; H, 4.68; N, 9.71; S, 7.37%. IR: ν(OH) 3449, ν(NH) 3299, δ(NH)1616, $\nu(C{=}N^1)$ 1593, $\nu(C{=}N^2)$ 1547, ν_s,ν_{as} (MoO_2) 935, 900. ^1H NMR: 9.67 (s, 1H, C*H*=N^1), 7.27–8.20 (doublet and triplets, 6H, $C_{10}H_6$), 7.02 (s, 1H, N^4H), 3.14 (q, 2H, S–CH_2), 1.39 (t, 3H, –CH_3), 3.65 (q, 2H, –C$^1H_2$), 1.16 (t, 3H, –C$^2H_3$).

1c: Cardinal red, >250 (dec), 190 mg (42%). *Anal.* Calc. for $C_{17}H_{21}MoN_3O_4S$ (459.37 g/mol): C, 44.45; H, 4.61; N, 9.15; S, 6.98. Found: C, 44.18; H, 4.46; N, 9.09; S, 6.52%. IR: ν(OH) 3441, ν(NH) 3214, δ(NH) 1616, $\nu(C{=}N^1)$ 1597, $\nu(C{=}N^2)$ 1547, ν_s,ν_{as}

(MoO_2) 946, 904. ^{1}H NMR: 9.67 (s, 1H, C*H*=N^1), 7.27–8.20 (doublet and triplets, 6H, $C_{10}H_6$), 7.01 (s, 1H, N^4*H*), 3.14 (q, 2H, S–C*H*$_2$), 1.40 (t, 3H, –C*H*$_3$), 3.54 (q, 2H, –C^1*H*$_2$), 1.51 (m, 2H, –C^2*H*$_2$), 0.83 (t, 3H, –C^3*H*$_3$).

1d: Orange, >250 (dec), 265 mg (56%). *Anal.* Calc. for $C_{18}H_{25}MoN_3O_4S$ (473.39 g/mol): C, 45.47; H, 4.92; N, 8.84; S, 6.74. Found: C, 45.72; H, 5.30; N, 8.81; S, 6.49%. IR: ν(OH) 3453, ν(NH) 3222, δ(NH) 1620, ν(C=N^1) 1597, ν(C=N^2) 1547, ν_s,ν_{as} (MoO_2) 946, 904. ^{1}H NMR: 9.67 (s, 1H, C*H*=N^1), 7.27–8.20 (doublet and triplets, 6H, $C_{10}H_6$), 7.02 (s, 1H, N^4*H*), 3.14 (q, 2H, S–C*H*$_2$), 1.39 (t, 3H, –C*H*$_3$), 3.57 (q, 2H, –C^1*H*$_2$), 1.48 (m, 2H, –C^2*H*$_2$), 1.32 (m, 2H, –C^3*H*$_2$), 0.86 (t, 3H, –C^4*H*$_3$).

2a: Stammel red, 233.3, 190 mg (38%). *Anal.* Calc. for $C_{21}H_{21}MoN_3O_4S$ (507.41 g/mol): C, 49.71; H, 4.17; N, 8.28; S, 6.32. Found: C, 49.38; H, 4.00; N, 8.24; S, 6.53%. IR: ν(OH) 3434, ν(C=N^1) 1593, ν(C=N^2) 1543, ν_s,ν_{as} (MoO_2) 939, 908. ^{1}H NMR: 9.69 (s, 1H, C*H*=N^1), 7.32–8.21 (doublet and triplets, 6H, $C_{10}H_6$), 7.21–7.35 (m, 5H, N^{4}C$_6$*H*$_5$), 3.05 (q, 2H, S–C*H*$_2$), 1.31 (t, 3H, –C*H*$_3$), 3.42 (s, 3H, –C^1*H*$_3$).

2b: Cardinal red, 232.1, 235 mg (45%). *Anal.* Calc. for $C_{22}H_{23}MoN_3O_4S$ (521.44 g/mol): C, 50.67; H, 4.45; N, 8.06; S, 6.15. Found: C, 50.72; H, 4.23; N, 8.07; S, 6.20%. IR: ν(OH) 3414, ν(C=N^1) 1593, ν(C=N^2) 1547, ν_s,ν_{as} (MoO_2) 942, 888. ^{1}H NMR: 9.76 (s, 1H, C*H*=N^1), 7.38–8.28 (doublet and triplets, 6H, $C_{10}H_6$), 7.27–7.41 (m, 5H, N^{4}C$_6$*H*$_5$), 3.15 (q, 2H, S–C*H*$_2$), 1.37 (t, 3H, –C*H*$_3$), 3.71 (q, 2H, –C^1*H*$_2$), 1.23 (t, 3H, –C^2*H*$_3$).

2c: Stammel red, 234.7, 115 mg (21%). *Anal.* Calc. for $C_{23}H_{25}MoN_3O_4S$ (535.47 g/mol): C, 51.59; H, 4.71; N, 7.85; S, 5.99. Found: C, 51.40; H, 4.44; N, 7.88; S, 5.97%. IR: ν(OH) 3422, ν(C=N^1) 1593, ν(C=N^2) 1543, ν_s,ν_{as} (MoO_2) 942, 885. ^{1}H NMR: 9.76 (s, 1H, C*H*=N^1), 7.38–8.28 (doublet and triplets, 6H, $C_{10}H_6$), 7.25–7.42 (m, 5H, N^{4}C$_6$*H*$_5$), 3.16 (q, 2H, S–C*H*$_2$), 1.38 (t, 3H, –C*H*$_3$), 3.60 (t, 2H, –C^1*H*$_2$), 1.58 (m, 2H, –C^2*H*$_2$), 0.93 (t, 3H, C^3*H*$_3$).

2d: Stammel red, 232.4, 110 mg (20%). *Anal.* Calc. for $C_{24}H_{27}MoN_3O_4S$ (549.49 g/mol): C, 52.27; H, 5.30; N, 7.62; S, 5.81. Found: C, 52.48; H, 5.01; N, 7.64; S, 6.02%. IR: ν(OH) 3260, ν(C=N^1) 1589, ν(C=N^2) 1543, ν_s,ν_{as} (MoO_2) 942, 888. ^{1}H NMR: 9.76 (s, 1H, C*H*=N^1), 7.39–8.28 (doublet and triplets, 6H, $C_{10}H_6$), 7.28–7.42 (m, 5H, N^{4}C$_6$*H*$_5$), 3.16 (q, 2H, S–C*H*$_2$), 1.38 (m, 3H, –C*H*$_3$), 3.65 (t, 2H, –C^1*H*$_2$), 1.55 (m, 2H, –C^2*H*$_2$), 1.38 (m, 2H, –C^3*H*$_2$), 0.93 (t, 3H, –C^4*H*$_3$).

3. Results and discussion

3.1. Some physical properties of the compounds

Hydrobromide forms of the ligands, which separated by precipitation of the reaction mixture, are bright yellow in color, whilst the free ligands are light yellow. The crystalline powders of H_2L^1 and H_2L^2 are soluble in common solvents. The reactions of the ligands with $MoO_2(acac)_2$ in a 1:1 molar ratio in selected alcohols yielded stable solid complexes corresponding to the general formula [MoO_2(L)ROH] (Fig. 1). The diamagnetic chelate complexes, **1a–d** and **2a–d**, are in the crystalline form, and they are soluble in alcohols and chlorinated hydrocarbons. The complexes are stable for at least 2 weeks in air.

3.2. IR and ^{1}H NMR spectra

The IR spectra of H_2L^1 and H_2L^2 clearly showed the stretching vibrations of the OH, N^{4}H, C=N^1 and N^4=C groups. In the IR spectra of the complexes, the ν(OH), one of the ν(NH) (for **1a–d**) and the ν(NH) (for **2a–d**) stretches are absent as a result of the deprotonation of the thiosemicarbazone ligands. The vibrations of the C=N^1 and N^4=C groups of the free thiosemicarbazones are shifted by *ca.* 8–27 cm^{-1} to lower frequencies on chelation. The spectra of the complexes contain the CH_2 and CH_3 stretching vibrations attributed to S-ethyl and coordinated alcohols, and also ν(OH) bands of the alcohols. The characteristic ν_s and ν_{as} bands of *cis*-MoO_2 are in the 885–912 and 935–955 cm^{-1} ranges.

The ^{1}H NMR spectra of the ligands showed the expected isomer peaks of azomethine (CH=N^1) and *S*-ethylprotons, and also N^{4}H$_2$ protons of H^{2}L^1 [21,29]. The chemical shifts of the naphthylidene ring protons of the ligands were observed an arrangement of doublet and triplet peaks between 7.19 and 8.18 ppm.

The signals of the isomers disappear on chelation, and only one singlet, triplet and quartet were recorded for the CH=N^1, –CH_3 and S–CH_2 protons, respectively. After chelation of the MoO_2^{2+} center, the CH=N^1 proton that is closer to the conjugated backbone of the thiosemicarbazone shifted to higher frequencies by 0.1–0.4 ppm, whilst the chemical shift values of the naphthylidene and ethyl protons are approximately the same as the free ligands. Because complex formation of the dibasic thiosemicarbazone ligands occurs synchronously with the deprotonisation of the 2-OH and N^{4}HR groups (Fig. 1), the phenoxy (of L^1 and L^2) and thioamide (of L^2) proton signals are absent in all the complex spectra. For the same reason, one singlet was observed at around 7 ppm in the spectra of **1a–d** instead of two singlet signals (at 5.11 and 4.78 ppm) appearing due to the *cis*- and *trans*-isomerism of N^{4}H$_2$ in the H$_2$L^1 spectra.

Other noticeable changes in chemical shifts were determined for five protons on the N^4-phenyl ring of **2a–d**. The doublet and triplets of these protons were recorded in a narrower range, *ca.* 0.15 ppm, while their chemical shifts are in a 0.33 ppm range (between 7.10 and 7.43 ppm) in the H$_2$L^2 spectra.

3.3. Crystallography

Single crystals of complexes **1b** and **2a**, suitable for X-ray diffraction studies, were grown by slow evaporation of an alcohol (L′) solution of the complex. Crystal parameters and refinement results of the complexes are summarized in Table 1.

The complex structures are formed by chelation of the doubly deprotonated thiosemicarbazones, having an ONN donor set which consist of a phenoxy oxygen atom and azomethine and thioamide nitrogen atoms. Two oxo-oxygens of molybdenum and an oxygen atom of an attached alcohol are also coordinated to the center. The oxygen atoms of ethanol (in **1b**) and methanol (in **2a**) are weakly coordinated with a Mo–O distance of 2.3727(13) and 2.4040(14) Å, respectively (Figs. 2 and 3). Considering the molybdenum centered bond distances and angles it can be easily seen that the molybdenum atoms of **1b** and **2a** are in three axis distorted octahedral environments (Tables 2 and 3). Compounds **1b** and **2a** have a *cis*-MoO_2 center and their geometric parameters are in the expected ranges compared with analogous molybdenum centric complexes of S-alkyl thiosemicarbazones [16,21,22,33].

Complex **1b** crystallizes in the monoclinic space group *C*2/*c* with *Z* = 8 (Fig. 2). One of the intermolecular hydrogen bonds (2.25 Å) ties the hydrogen atom (H3A) of the NH group and the oxo-oxygen (O3). In another interaction, the hydroxyl proton (H1) of the coordinated ethanol and the nitrogen atom (N2) are involved (Fig. 4.). In this way, a 3D-structure of complex **1b** is generated by the propagation of these hydrogen bonds in the form of a bifurcated arrangement.

The molybdenum complex of L^2 (**2a**) crystallizes from methanol in the monoclinic space group $P2_1/n$. The hydroxyl proton of the coordinated methanol participates in an intermolecular interaction and results in a hydrogen bond, 1.99(3) Å in length (Fig. 5). Pairs of these hydrogen bonds connect two molecules into a dimer in which S-ethyl groups of the complex structures are outstretched in opposite directions and the chelate rings are in parallel planes.

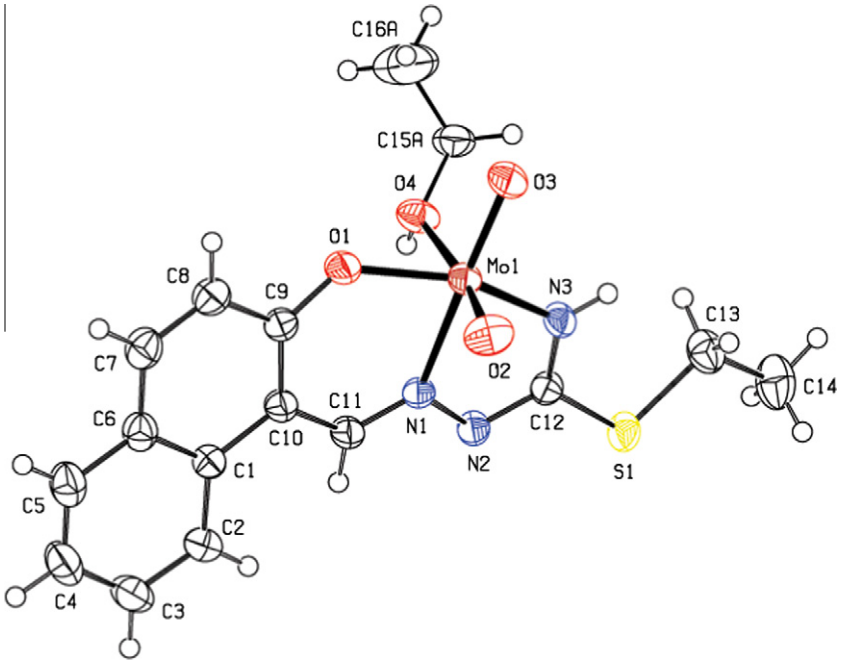

Fig. 2. The molecule of **1b** with the atom numbering scheme. Displacement ellipsoids for non-H atoms are drawn at the 50% probability level. The minor component of the disordered part has been omitted for clarity.

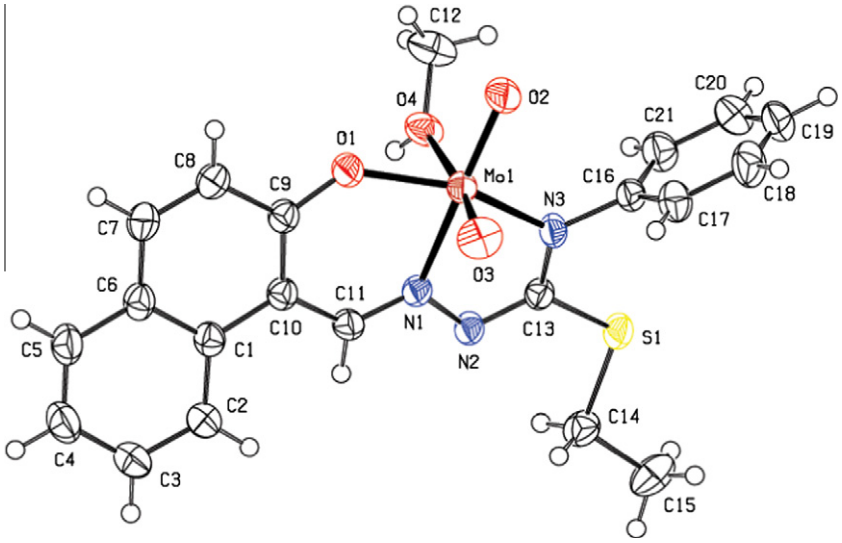

Fig. 3. The molecule of **2a** with the atom numbering scheme. Displacement ellipsoids for non-H atoms are drawn at the 50% probability level.

Furthermore, for both of **1b** and **2a**, weak intermolecular C–H···π interactions contribute to the stabilization of the crystal packing (see for details; Table 4).

3.4. Electrochemical studies

The redox properties of the ligands ($H_2\mathbf{L^1}$ and $H_2\mathbf{L^2}$) and their dioxomolybdenum(VI) complexes (**1b** and **2a**) were studied using CV and SWV measurements in DCM containing TBAP as the supporting electrolyte on a Pt electrode. Table 5 lists the assignments of the redox couples and the electrochemical parameters, which included the half-wave peak potentials ($E_{1/2}$), anodic to cathodic peak potential separation (ΔE_p), and ratio of the anodic to cathodic peak currents (I_{pa}/I_{pc}). $E_{1/2}$ values are in agreement with the reported data for redox processes in similar O–N–S complexes in the literature [34–42].

The ligands $\mathbf{L^1}$ and $\mathbf{L^2}$ indicate similar voltammetric responses with small potential shifts due to the different substituents. Within the electrochemical window of TBAP/DCM, they undergo a one-electron irreversible oxidation (two oxidations for $\mathbf{L^1}$) and a one-electron irreversible reduction couple (Fig. 6). It is observed that the redox potentials of $\mathbf{L^2}$ shift to positive potentials due to the different substituents of the ligand. When one of the hydrogen atoms of the NH_2 group was exchanged with a phenyl group to form $\mathbf{L^2}$, the redox potentials shift to positive potentials due to the higher electron withdrawing ability of the phenyl group with respect to

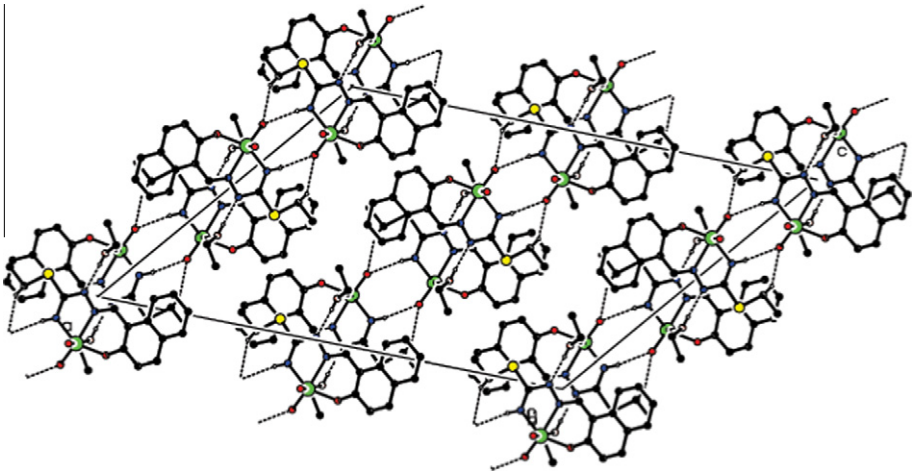

Fig. 4. The packing and hydrogen bonding interactions of the compound **1b** viewed down the *b*-axis. H atoms not participating in hydrogen bonding and the minor component of the disordered part have been omitted for clarity.

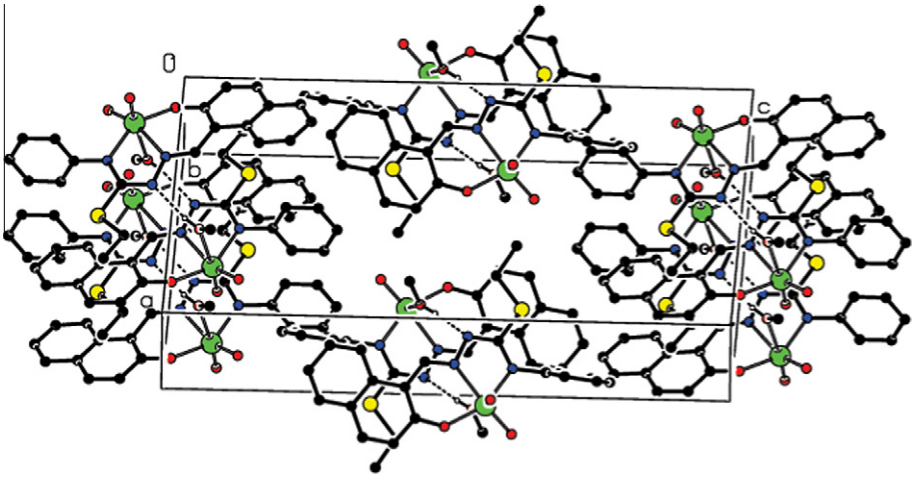

Fig. 5. A general view of the packing and hydrogen bonding interactions of the compound **2a**. H atoms not participating in hydrogen bonding have been omitted for clarity.

Table 5
Voltammetric data of the compounds.

Complex		Ligand oxd.'s		$M^{IV}O_2/M^{V}O_2$	Ligand red.
L[1]	$E_{1/2}$ vs. SCE[a]	1.46	0.98		−1.88
	ΔE_p (mV)[b]		450		
	I_{pa}/I_{pc}[c]		0.17		
L[2]	$E_{1/2}$ (V)[a]		1.12		−1.52
	ΔE_p (mV)[b]		400		80
	I_{pa}/I_{pc}[c]		0.15		0.30
1b	$E_{1/2}$[a]		1.17	−0.86	−1.52
	ΔE_p (mV)[b]			180	185
	I_{pa}/I_{pc}[c]			0.22	0.56
2a	$E_{1/2}$[a]		1.27	−0.80	−1.48
	ΔE_p (mV)[b]		110	153	210
	I_{pa}/I_{pc}[c]		0.15	0.25	0.42

[a] $E_{1/2} = (E_{pa} + E_{pc})/2$ at 0.100 V s^{-1}.
[b] $E_p = E_{pa} + E_{pc}$ at 0.100 V s^{-1}.
[c] I_{pa}/I_{pc} for reduction, I_{pc}/I_{pa} for oxidation processes at 0.100 V s^{-1} scan rate.

hydrogen. Although the irreversible reduction process of these ligands was reported in the literature for similar ligands [40–42], the oxidation processes of the ligands are rarely reported [42].

Coordination of the ligands shifts the redox potential of the ligands to positive potentials due to the electron deficient character of the dioxomolybdenum (VI) center (Fig. 7).

Complexes **1b** and **2a** give a metal-based one-electron irreversible redox couple (at −0.5 V for **1b** and at −0.55 V for **2a**) in addition to the ligand-based redox processes. The free ligands do not exhibit a redox process in the potential range where the molybdenum reductions are observed. The values of $E_{1/2}$ are significantly influenced by the central metal ions, the nature of the substituents on the thiosemicarbazone ligands and the electronic character of the ligands, which are important factors in the control of redox potentials. Even though the ΔE_p values of **1b** and **2a** were in the quasi-reversible range, especially at very slow scan rates, the very small I_{pa}/I_{pc} values and the deviation of I_p vs. $v^{1/2}$ from linearity may assign the irreversible character of the redox processes to the chemical reactions succeeding the electron transfer processes. Due to the chemical reactions succeeding the reduction redox processes, the CV of **1b** gives oxidation waves at −0.20, 0.10, 0.44 and 1.15 V, assigned to the chemical reaction products during the reverse potential scans. Similar waves were also recorded with complex **2a**. When only the potential range from −0.5 to 1.6 V was scanned, without a negative potential scan, these waves

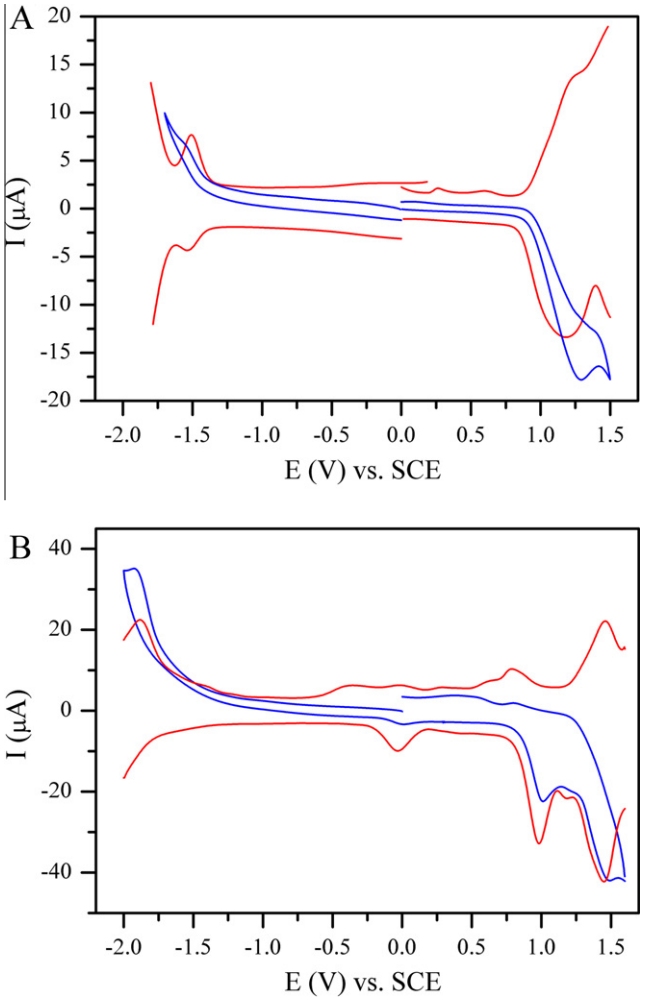

Fig. 6. CVs and SWV of the ligands at 0.100 V s^{-1} scan rate on Pt in DCM/TBAP. **(A)** L^2 and (B) L^1 (SWV parameters: pulse size = 100 mV; Frequency: 25 Hz).

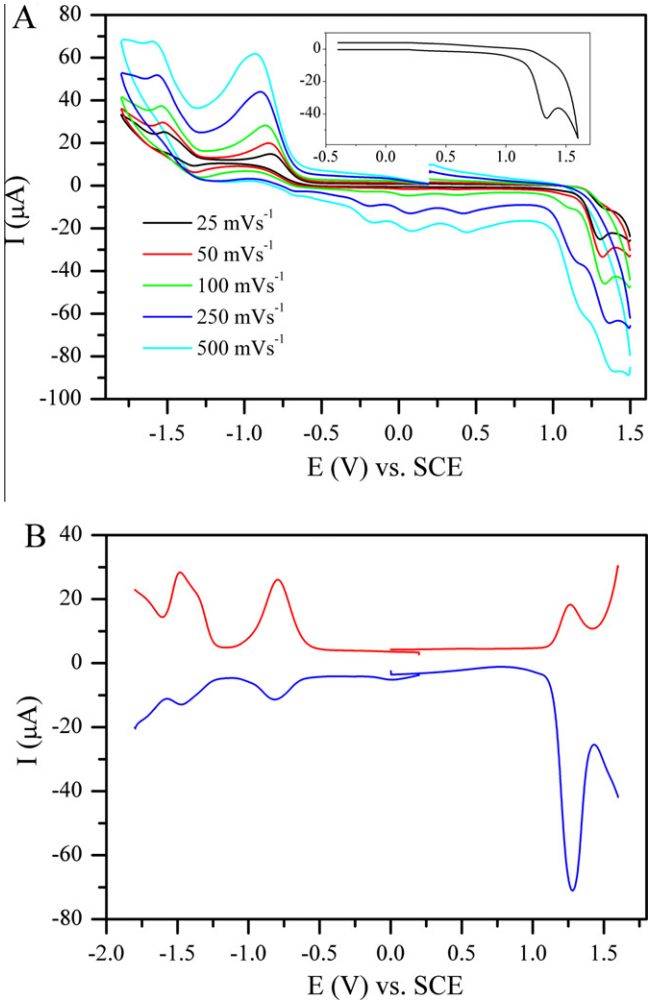

Fig. 7. CV (inset: positive potential scan 0.100 V s^{-1} scan rate) (**A**) and SWV (**B**) of **2a** at various scan rates on Pt in DCM/TBAP. (SWV parameters: pulse size = 100 mV; Frequency: 25 Hz).

disappeared, which supports the assignment of these waves to the product of the chemical reaction succeeding the reduction processes of the complexes. It is to be noted here that reductions of dioxomolybdenum(VI) complexes in aprotic solvents are generally irreversible [43–45]. This indicates that the electrochemical reductions are followed by chemical reactions. In general, the initial reduction product is a dioxomolybdenum(V) species which undergoes loss of an oxo group and/or dimer formation [40–45].

3.5. Spectroelectrochemical studies

In situ spectroelectrochemical studies were employed to determine the spectra of the electrogenerated species of the dioxomolybdenum(VI) complexes and to assign the redox processes in the CVs of the complexes. Since Mo(VI) has a $4d^0$ electronic configuration, the initial spectrum under an open-circuit potential is dominated by ligand-to-metal charge transfer (LMCT) and intraligand transitions. Fig. 8 shows the *in situ* UV–Vis spectral changes of **2a** as a representative of the dioxomolybdenum(VI) complexes during the controlled potential reductions and oxidation processes. Under an applied potential of −1.0 V, the broad LMCT band at 560 nm decreases in intensity without shift, while the intraligand transition band at 308 nm decreases in intensity with a red shift to 327 nm. At the same time, a sharp new band is observed at 390 nm (Fig. 8A). Shifting of the intraligand transition band at 308 nm and the change in the position of the LMCT band indicate a metal-based redox process and the couple is assigned to the $[Mo^{VI}O_2(L^2)MeOH]/[Mo^{V}O_2(L^2)MeOH]^{-1}$ process. Well-defined isosbestic points at 350 and 413 nm demonstrate that the reduction proceeds to give a single, reduced species. Fig. 8B illustrates the spectral changes during the ligand-based reduction process. During the −1.80 V potential application, while the bands at 327 and 390 nm remain unchanged, two new bands are observed at 300 and 445 nm. The spectroscopic changes given in Fig. 8C are characteristic for the decomposition of the complex during oxidation, because all bands decreases in intensity and no clear isosbestic point is recorded under the applied potential at 1.50 V. The color changes of the compounds during the redox processes were recorded using *in situ* colorimetric measurements (Fig. 8D). Without any potential application, the solution of $[Mo^{VI}O_2(L^2)MeOH]$ is red ($x = 0.4728$ and $y = 0.4186$). As the potential is stepped from 0 to −1.70 V, the color of the neutral $[Mo^{VI}O_2(L^2)MeOH]$ starts to change and a light green color ($x = 0.3439$ and $y = 0.4694$) is seen during the first reduction and then a yellow color ($x = 0.4339$ and $y = 0.4694$) is obtained at the end of the reduction. During the oxidation process, the color of the solution changes from red to light yellow ($x = 0.3952$ and $y = 0.416$). Measurement of the *xyz* coordinates allows quantification of each color of the redox species, which is very important in deciding their possible electrochromic application.

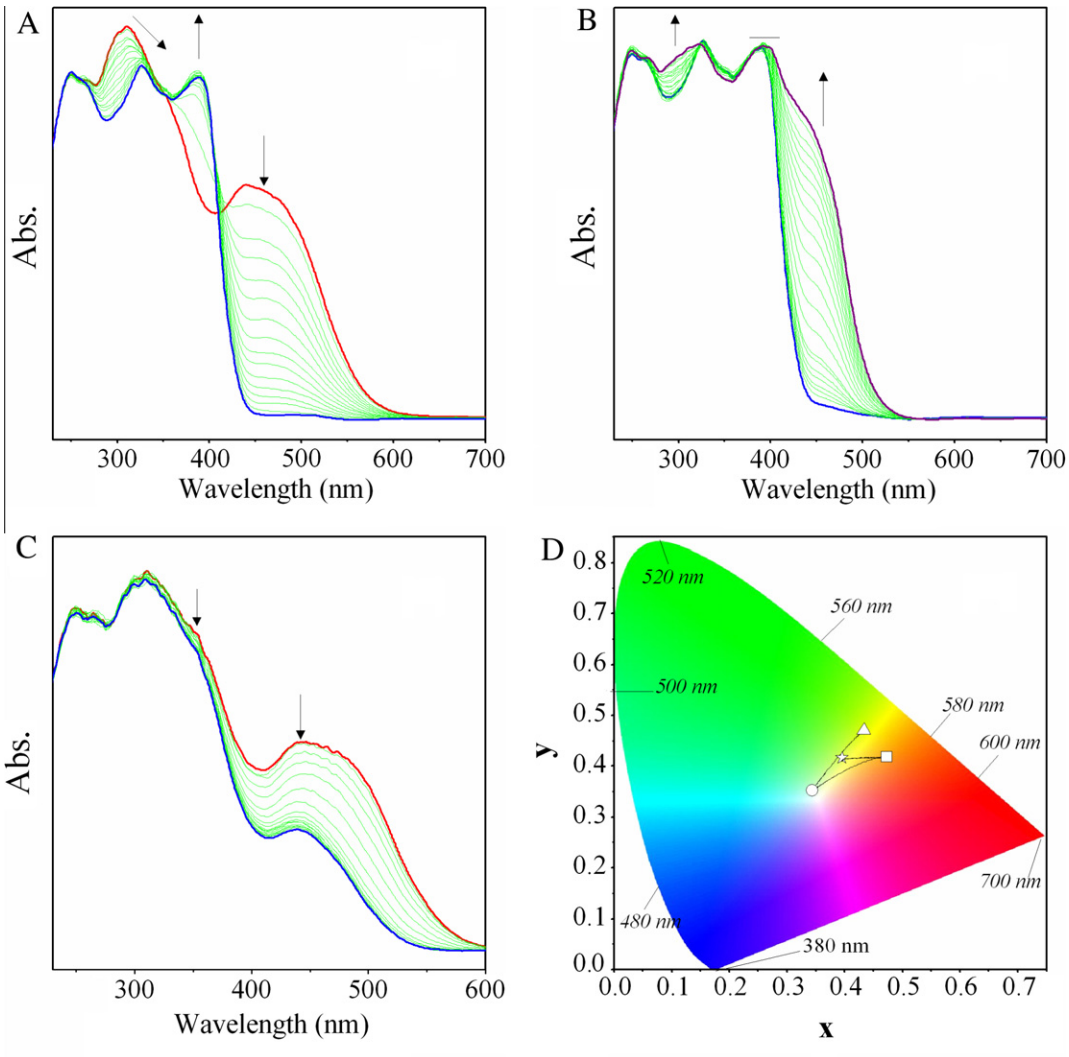

Fig. 8. *In situ* UV–Vis spectral changes of **2a**. (A) $E_{app} = -1.00$ V. (B) $E_{app} = -1.80$ V. (C) $E_{app} = 1.50$ V. (D) Chromaticity diagram of **2a**. (Each symbol represents the color of electrogenerated species; □ : $[Mo^{VI}O_2(L^2)MeOH]$, ○: $[Mo^{V}O_2(L^2)MeOH]^{-1}$, △: $[Mo^{VI}O_2(L^2)^{-1}MeOH]^{-2}$, ☆: $[Mo^{VI}O_2(L^2)^{+1}MeOH]^{+1}$.

4. Conclusion

As known, the *cis*-MoO_2 center in the chelate form shows a catalytic function in net oxygen atom transfer (OAT), and its ability varies in relation to the chelating ligand type and substituents of the ligand. For this purpose, many dioxomolybdenum complexes with various 2-hydroxy-arylidene thiosemicarbazones have been investigated. However, S-alkyl thiosemicarbazone derivatives have been the subject of a limited number of reports [14–16,20–22], and there is only one study on S-ethyl thiosemicarbazones [33].

In this study, a series of *cis*-MoO_2 complexes (**1a–d** and **2a–d**) with two S-ethyl-thiosemicarbazones, which are potential catalysts for various enzymes and OAT reactions, were synthesized. Structural analysis of **2a–d** confirmed that the N^4 thioamide nitrogen atom has reaction capability despite the steric bulk of the phenyl ring. Crystallographic data of **1b** and **2a** showed the remarkable role of the OH protons of the bonded alcohols in relatively strong intermolecular hydrogen bonds.

Voltammetric and spectroelectrochemical studies show that while the free ligands give a one electron reduction and a one electron oxidation redox process, the dioxomolybdenum(VI) complexes **1b** and **2a** give an irreversible metal-based one electron reduction process in addition to the irreversible ligand reduction and oxidation processes. The redox potentials of the ligands shift to positive potentials after coordination to the dioxomolybdenum(VI) center. The data clearly indicate that the substituents of the ligands also affect the redox processes of the ligands and their complexes. Additionally, a definite determination of the colors of the electrogenerated anionic and cationic form of the complexes is important in deciding their possible electrochromic application.

Supplementary data

CCDC 753393 and 746352 contain the supplementary crystallographic data for complex **1b** ($C_{16}H_{19}N_3O_4MoS$) and complex **2a** ($C_{21}H_{21}N_3O_4MoS$). These data can be obtained free of charge via http://www.ccdc.cam.ac.uk/conts/retrieving.html, or from the Cambridge Crystallographic Data Centre, 12 Union Road, Cambridge CB2 1EZ, UK; fax: (+44) 1223-336-033; or e-mail: deposit@ccdc.cam.ac.uk.

Acknowledgments

This present work was supported by the Research Fund of Istanbul University, Project No. 810. The authors thank Dr. Gülşah Yurdakul (Istanbul University, IA Laboratory, Istanbul) for her useful assistance during X-ray diffraction data collection.

References

[1] R.H. Holm, Chem. Rev. 87 (1987) 1401.
[2] R.S. Pilato, E.I. Stiefel, In: J. Reedijk, E. Bouwman, Bioinorganic Catalysis, second ed., Marcel Dekker, New York, 1999 (Chapter 6).
[3] C.R. Cornman, K.L. Jantzi, J.I. Wirgau, T.C. Stauffer, J.W. Kampf, P.D. Boyle, Inorg. Chem. 37 (1998) 5851.
[4] J.U. Mondal, J.G. Zamora, M.D. Kinon, F.A. Schultz, Inorg. Chim. Acta 309 (2000) 147.
[5] R. Dinda, P. Sengupta, S. Ghosh, H. Mayer-Figge, W.S. Sheldrick, J. Chem. Soc., Dalton Trans. (2002) 4434.
[6] J.P. Donahue, C.R. Goldsmith, U. Nadiminti, R.H. Holm, J. Am. Chem. Soc. 120 (1998) 12869.
[7] C.E. Webster, M.B. Hall, J. Am. Chem. Soc. 123 (2001) 5820.
[8] B.E. Scbultz, S.F. Gbeller, M.C. Muetterties, M.J. Scott, R.H. Holm, J. Am. Chem. Soc. 115 (1993) 2714.
[9] A. Rana, R. Dinda, S. Ghosh, A.J. Blake, Polyhedron 22 (2003) 3075.
[10] C. Whiteoak, G.J.P. Britovsek, V.C. Gibson, A.J.P. White, J. Chem Soc., Dalton Trans. (2009) 2337.
[11] U. Küsthardt, R.W. Albach, P. Kiprof. Inorg. Chem. 32 (1993) 1838.
[12] J.M. Berg, K.O. Hodgson, A.E. Bruce, J.L. Carbin, N. Pariyadath, E.I. Stiefel, Inorg. Chim. Acta 90 (1984) 25.
[13] S. Purohit, A.P. Koley, L.S. Prasad, P.T. Manoharan, S. Ghosh. Inorg. Chem. 28 (1989) 3735.
[14] E.Z. Iveges, V.M. Leovac, G. Pavlovic, M. Penavic, Polyhedron 11 (13) (1992) 1659.
[15] K.M. Szecsenyi, V.M. Leovac, E.Z. Iveges, L. Arman, A. Kovacs, G. Pokol, S. Gal, Thermochim, Acta 291 (1–2) (1997) 101.
[16] Z.D. Tomic, A. Kapor, A.Z. Miric, V.M. Leovac, D. Zobel, S.D. Zaric, Inorg. Chim. Acta 360 (2007) 2197.
[17] V. Vrdoljak, M. Cindric, D. Milic, D. Matkovic-Calogovic, P. Novak, B. Kamenar, Polyhedron 24 (2005) 1717.
[18] M. Cindric, V. Vrdoljak, N. Strukan, B. Kamenar, Polyhedron 24 (2) (2005) 369.
[19] E.B. Seena, M.R.P. Kurup, Polyhedron 26 (2007) 3595.
[20] Y.D. Kurt, G.S. Pozan, İ. Kızılcıklı, B. Ülküseven, Russ. J. Coord. Chem. 33 (11) (2007) 844.
[21] I. Kızılcıklı, S. Eğlence, A. Gelir, B. Ülküseven, Transition Met Chem 33 (2008) 775.
[22] B.İ. Ceylan, Y.D. Kurt, B. Ülküseven, J. Coord. Chem. 62 (5) (2009) 757.
[23] Rigaku/MSC, CrystalClear, Rigaku/MSC Inc., The Woodlands, TX, USA, 2006.
[24] R.H. Blessing, Acta Cryst A51 (1995) 33.
[25] A. Altomare, M.C. Burla, M. Camalli, G.L. Cascarano, C. Giacovazzo, A. Guagliardi, A.G.G. Moliterni, G. Polidori, R. Spagna, J. Appl. Cryst. 32 (1999) 115.
[26] G.M. Sheldrick, Acta Cryst A64 (2008) 112.
[27] L.J. Farrugia, J. Appl. Cryst. 30 (1997) 565.
[28] A.L. Spek, J. Appl. Cryst. 36(2003) 7.
[29] C. Yamazaki, Can. J. Chem. 53 (1975) 614.
[30] S.G. Shova, M.A. Yampol'skaya, B.G. Zemskov, K.I. Turte, I.N. Ivleva, Russ. J. Inorg. Chem. 30 (9) (1985) 1312.
[31] V.M. Leovac, Lj.S. Jovanović, J.L. Bjelica, V.I. Cesljevic, Polyhedron 8 (1989) 135.
[32] V. Vrdoljak, M. Cindric, D. Matkovıc-Calogovic, B. Prugovecki, P. Novak, B. Kamaner, Z. Anorg. Allg. Chem. 631 (2005) 928.
[33] B.İ. Ceylan, Y.D. Kurt, B. Ülküseven, Rev. Inorg. Chem. 29 (1) (2009) 49.
[34] M. Kandaz, İ. Yılmaz, S. Keskin, A. Koca, Polyhedron 21 (2002) 825.
[35] M. Kandaz, A. Koca, A.R. Özkaya, Polyhedron 23 (2004) 1987.
[36] M. Kato, K. Nakajima, Y. Yoshikawa, M. Hirotsu, M. Kojima, Inorg. Chim. Acta 311 (2000) 69.
[37] P. Barbaro, C. Bianchini, G. Scapacci, D. Masi, P. Zanello, Inorg. Chem. 33 (1994) 3180.
[38] A.P. Rebolledo, O.E. Piro, E.E. Castellano, L.R. Teixeira, A.A. Batista, H. Beraldo, J. Mol. Struct. 794 (2006) 18.
[39] R.M. El-Shazly, G.A.A. Al-Hazmi, S.E. Ghazya, M.S. El-Shahawi, A.A. El-Asmya, Spectrochim. Acta A 61 (2005) 243.
[40] A.I. Matesanz, J. Mosa, I. Garćia, C. Pastor, P. Souza, Inorg. Chem. Commun. 7 (2004) 756.
[41] A. Arquero, M.A. Mendiola, P. Souza, M.T. Sevilla, Polyhedron 15 (1996) 1657.
[42] D. Mishra, S. Naskar, M.G.B. Drew, S.K. Chattopadhyay, Inorg. Chim. Acta 359 (2006) 585.
[43] A.S. Attia, S.F. El-Mashtoly, M.F. El-Shahat, Polyhedron 22 (2003) 895.
[44] Y. Sui, X. Zeng, X. Fang, X. Fu, Y. Xiao, L. Chen, M. Li, S. Cheng, J. Mol. Catal. A: Chem. 270 (2007) 61.
[45] A. Rana, R. Dinda, P. Sengupta, S. Ghosh, L.R. Falvello, Polyhedron 21 (2002) 1023.